

## Nickel oxide-gadolinium doped ceria synthesized by new methods as anodes material for solid oxide fuel cells

S. Ghamari Arbati <sup>1</sup>, M. Ranjbar <sup>\*1</sup>, A. Babaei <sup>2</sup>

<sup>1</sup>Department of Chemical Technologies, Iranian Research Organization for Science and Technology (IROST)

<sup>2</sup>University of Tehran- School of Metallurgy and Materials Engineering

### Article Information

Article History:

Received:

13 Aug 2022

Received in revised form:

04 Oct 2022

Accepted:

18 Oct 2022

### Keywords

Microstructures  
three-phase boundaries  
electrochemical performance  
Ni(II) complex  
SOFC

### Abstract

In this study, nickel oxide-gadolinium doped ceria, NiO–GDC, composite powder was synthesized by the sol-gel method with a new Ni(II) complex. A new Ni(II) complex, chemical formula  $[\text{Ni}(\mu\text{-L})_n(\text{NO}_3)_2]$ ,  $\text{L} = \text{N}'\text{-(pyridine-2-yl)methylene}$  isonicotinohydrazide), was used as a new precursor. The new Ni(II) complex was prepared by a reaction between ligand, L, and  $\text{Ni}(\text{NO}_3)_2 \cdot 6\text{H}_2\text{O}$  using the hydrothermal method. Then the NiO–GDC powders were synthesized using  $\text{Ce}(\text{NO}_3)_3 \cdot 6\text{H}_2\text{O}$ , and  $\text{Gd}(\text{NO}_3)_3 \cdot 6\text{H}_2\text{O}$ , and the as-synthesized new Ni(II) complex  $[\text{Ni}(\mu\text{-L})_n(\text{NO}_3)_2]$  with the sol-gel method. The NiO–GDC powder was modified to increase the performance of solid oxide fuel cells (SOFCs) operating at intermediate temperatures (600–800 °C) by increasing the three-phase boundary region in the anode. Finally, the NiO–GDC anode powders prepared with the new precursor were compared with the NiO–GDC anode powders synthesized from metal nitrates as a precursor. The results showed that the modified NiO–GDC anode had more three-phase boundaries, TPB, a more uniform microstructure, a higher specific surface area, and a porous structure that effectively improved the electrochemical performance of the electrode. SOFC half-cell resistance with this high-performance anode decreased by 85 % at 800 °C compared to conventional half-cells.

## 1 Introduction

Fuel cells have several potential advantages in produce electrical energy such as higher productivity, lower emissions, and developed power density [1].

Solid oxide fuel cells (SOFCs) and proton electrolyte membrane fuel cells (PEMFCs) are the most favored fuel cell technologies [2]. SOFCs are divided into two main types based on their operating temperature: high-temperature SOFCs, and low-temperature or

\*Corresponding Author: : marandjbar@irost.ir

intermediate-temperature SOFCs (IT-SOFCs) [3,4]. With the many problems encountered in commercializing high-temperature SOFCs, IT-SOFCs operating at 450–800 °C recently have possessed significant attention [1,5]. Therefore, various groups around the world are involved in developing materials used in anodes for IT-SOFCs [2, 5]. Anodes comprised of Gadolinium-doped ceria (GDC) are considered to be one of the most promising electrodes for use in IT-SOFCs. Ceramic electrodes for fabricating an anode body are comprised of a complex of two or more components, including conducting a precursor containing a metallic electrode material and electrolyte material [6]. The NiO nanostructures are introduced as a P-type semiconductor with a stable wide bandgap (3.6–4.0 eV) [7]. Nickel oxides are very popular in the fabrication of electrodes in SOFCs because of special features such as electrically conductive, highly insoluble and exceptionally thermally stable [6]. The sol-gel method for the synthesis of NiO-GDC anodes shows a lot of advantages like high phase purity, good compositional homogeneity, increase porosity, limited nickel agglomeration at high temperature, and high surface activity of the resulting powder [8]. The most common synthesis methods based on chemical reactions for NiO-GDC powders are solution combustion synthesis, polymeric complexing method, and co-precipitation [9]. In this research work, the preparation of NiO-GDC powder through the sol-gel method, using the new Ni (II) Schiff -base complex, has been carried out. With that in mind, the anode performance is mainly contingent on its fabrication process, fine particle sizes, optimized anode microstructure, and the resulting microstructure; therefore, it is essential for enhancing cell performance [6]. The interconnectivity between the NiO and GDC particles, the amount of porosity, and the length of the triple-phase boundaries (TPBs) determine the electrochemical performances of the anode [9]. Recently, Manthiram et al. improved the electrochemical performance of NiO-GDC through structural optimization. Their comparison

of the modified and conventional NiO-GDC anodes with the same porosity showed that the power densities of the modified NiO-GDC anode is three times more than that of the conventional anode [10]. In another study, highly porous NiO-GDC powders were synthesized by a one-pot glycine nitrate process [9]. The NiO-GDC anode with high porosity and best dispersion of Ni and GDC particles and increased power density was obtained through optimization [9]. Some researchers found that during the optimization process, the modification of the microstructure had an important role in the anode polarization resistance and electrochemical activity [11]. Hence, further improvements in the NiO-GDC anodic property will result in improved structures of anode powders. In this paper, we present an approach to enlarge the TPB area of the SOFC anodes by surface modification of the anode powder, which can be applied as anode material for IT-SOFC. The NiO-GDC anode powder has been synthesized by a new Ni(II) complex with the chemical formula  $[\text{Ni}(\mu\text{-L})]_n(\text{NO}_3)_2$ , ((L= (pyridine-2-yl)methylene)isonicotinohydrazide) as a new precursor, which increases the length of the three-phase boundaries and improves the electrochemical performance. The thermal stability, porosity and electrochemical behavior of the modified NiO-GDC are compared with the conventional NiO-GDC prepared by nickel nitrate salt as previously reported [12].

---

## 2. Experimental

### 2.1 Preparation of the metal complex of the Schiff base

The N'-(pyridine-2-yl)methylene)isonicotinohydrazide, L, was prepared according to the procedure found in the literature [13]. The schematic of the synthesis methods employed in the present work for the synthesis of the ligand is shown in Fig. 1. For the synthesis of the  $[\text{Ni}(\mu\text{-L})]_n(\text{NO}_3)_2$  complex, the Schiff base ligand

(L, 1 mmol) and the  $\text{Ni}(\text{NO}_3)_2 \cdot 6\text{H}_2\text{O}$  (1 mmol) was dissolved in the Ethanol solvent. This solution was transferred into a thermal bomb for 72 hours at 170 °C. The resulting precipitate was collected and washed with ethanol and distilled water, respectively. The Ni(II)

complexes were a dark green color. Yields of the first crops of the compound were 75 %. Elemental analysis (%): Calc for  $\text{C}_{12}\text{H}_{10}\text{N}_6\text{NiO}_7$ : C, 35.25; H, 2.46; N, 20.55; Ni, 14.35; Found: C, 35.25; H, 2.46; N, 20.55.

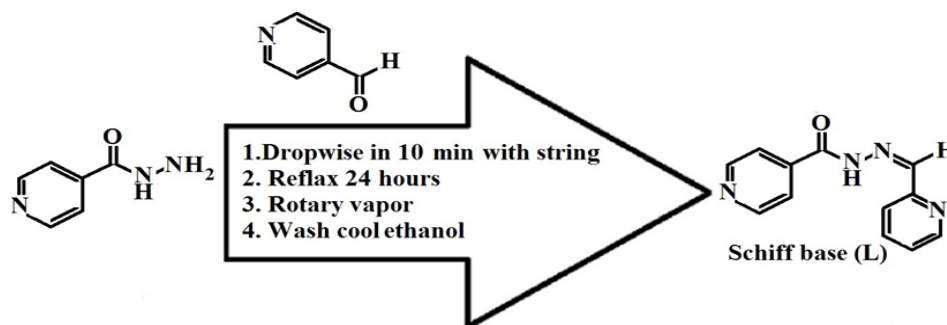


Fig. 1. Schematic of the synthesis methods for Schiff base (L).

## 2.2 Preparation of modified NiO-GDC

The conventional NiO-GDC was synthesized by a sol-gel method without the new precursor, according to our previous work [12]. For the preparation of the modified NiO-GDC composite powder,  $\text{Ce}(\text{NO}_3)_3 \cdot 6\text{H}_2\text{O}$  (99.99%, Merck),  $\text{Gd}(\text{NO}_3)_3 \cdot 6\text{H}_2\text{O}$  (99.99%, Aldrich),  $[\text{Ni}(\mu\text{-L})]_n(\text{NO}_3)_2$ , ethylene glycol and anhydrous citric acid (Mw = 192.124 g/mol) (Merck) were used as the starting materials. The  $\text{Ce}(\text{NO}_3)_3 \cdot 6\text{H}_2\text{O}$ ,  $[\text{Ni}(\mu\text{-L})]_n(\text{NO}_3)_2$ , and  $\text{Gd}(\text{NO}_3)_3 \cdot 6\text{H}_2\text{O}$  were dissolved in deionized water separately; this was followed by the addition of ethylene glycol and citric acid dissolved in deionized water as the chelating agents. The resulting clear solutions were mixed for 3 h at 90 °C and then concentrated via the evaporation of the solvent at 100 °C until it turned into a thick, viscous gel. The resulting gel was dried in an oven at 110 °C for 3 hours; Then, the ensuing products were collected and converted into powders by simple grinding, using a mortar and pestle; finally, they were annealed in a furnace and then calcined at 600 °C for 6h to obtain the modified NiO-GDC composite.

## 2.3 Characterization

All solutions were prepared using double distilled water. Elemental analyses were performed using a CHN Heraeus CHN-O-Rapid analyzer for C, H, and N. The Fourier transform infrared (FT-IR) spectra were recorded on a Bruker tensor 27 spectrometer in the range 400– 4,000  $\text{cm}^{-1}$  using the KBr disk technique. The thermal analysis of the as-combusted precursor was characterized by TG/DTA analysis using a PL-StA 1500 equipped thermal analyzed in flowing Argon at a heating rate of 10 °C/min. The Brunauer–Emmett–Teller (BET) measurement was carried out to obtain the surface area of the as-prepared and calcined powders by using a Belsorp mini II made in Japan. The crystalline nature and phase purity were examined using powder X-ray diffraction (XRD) technique (X'Pert Pro, INEL Equinox 3,000, X-ray diffractometer) with  $\text{Cu-K}\alpha$  radiation. The crystallite sizes were determined using the Scherrer equation [14]. The morphology, particle size, and distribution of the powders were analyzed by both scanning electron microscopy (SEM, JEOL 6460 LV) attached and transmission electron microscopy (TEM, JEOL JEM 2000 EX).

## 2.4 Fabrication of the half-cell and testing process

A three-electrode configuration was used for the electrochemical measurements of the asymmetric cells, which was similar to that reported in another study [15]. The electrolyte discs were prepared by the die-pressing of 8 mol %  $Y_2O_3-ZrO_2$  powder (YSZ, Tosoh, Japan), which was followed by sintering at  $1500^\circ C$  for 4 h. The diameter and thickness of the electrolyte were 19 and 0.9 mm, respectively. The surface of the electrolyte pellets was roughened by grinding it with sandpaper to increase the contact between the electrode and electrolyte. The conventional and modified NiO-GDC powders were mixed with an ink vehicle (Fuel cell Materials, USA); and applied to the YSZ pellets by the slurry painting method; this was followed by sintering at  $1380^\circ C$  for 2 h in air. The electrode area was  $0.4\text{ cm}^2$  after sintering. A Pt paste was applied as the counter and reference electrodes. The electrochemical performance of the cermet anodes was characterized by the electrochemical impedance spectroscopy (EIS) technique using a PARStAT 2273 potentiostat/galvanostat in the frequency range of 0.1 Hz to 0.1 MHz and signal amplitude of 10 mV.

The EIS spectra were recorded at  $650-800^\circ C$  with  $50^\circ C$  intervals using wet hydrogen/nitrogen (50:50 vol. ratio) gas as the fuel and ambient air as the oxidant. The impedance response of the modified NiO-GDC anode was measured and compared with that of the conventional Ni-GDC anode. All density functional theory (DFT) calculation was executed by the Gaussian 03W program and with the B3lyp-Lan-12dz basic set.

## 3. Results and discussion

The reaction of the Schiff base (L) with the  $Ni(NO_3)_2 \cdot 6H_2O$  in the Ethanol solvent using the thermal bomb at  $170^\circ C$  leads to the formation of the  $[Ni(\mu-L)]_n(NO_3)_2$  complex. A graphical geometry of coordination environment around the  $[Ni(\mu-L)]_n(NO_3)_2$  complex is shown in Fig. 2.

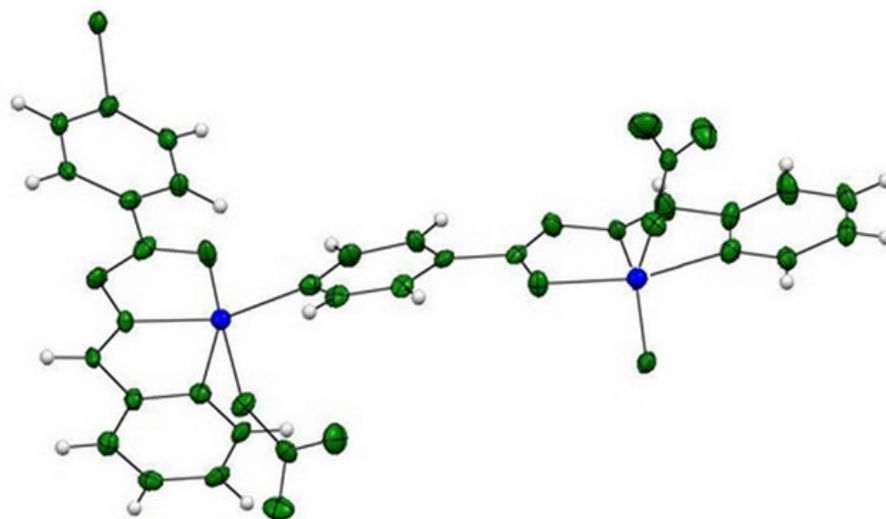


Fig. 2. The molecular structure of the  $[Ni(\mu-L)]_n(NO_3)_2$  complex

In Fig. 3a, we propose a structure based on the experimental analysis result and the DFT calculation. After geometrical optimization [16, 17] for the proposed structure, we can extract the results described in this section. Fig. 3b shows the boundary orbitals, HOMO and LUMO, along with their corresponding bandgap and energy that are calculated by DFT-B3lyp-land-2d. According to the calculations, the bandgap value is a meager and about 0.25 eV, which indicates the meager energy difference between the boundary orbitals, HOMO and LUMO. This low value enables the electron transfer from the HOMO to the LUMO orbitals with a minimal amount of energy, which would happen at high wavelengths. The three-dimensional

schematic representation of the total electron density of the  $[\text{Ni}(\mu\text{-L})_n(\text{NO}_3)_2]$  complex is presented in Fig. 3c, where the highest electron density is concentrated at the metallic center. A two-dimensional representation of the total electron density of the central part of the  $[\text{Ni}(\mu\text{-L})_n(\text{NO}_3)_2]$  complex can be observed in Fig. 3d, which shows the nearly uniform distribution of density around the metallic center and the equatorial region. In Fig. 3e, nickel has a partial charge of +0.51, and the atoms coordinated to it have a negative partial charge whose amount is lower than the free Schiff base, which in turn is evidence of the ligand-to-metal charge-transfer (LMCT) charge transportation from the ligands toward nickel at the metallic center.

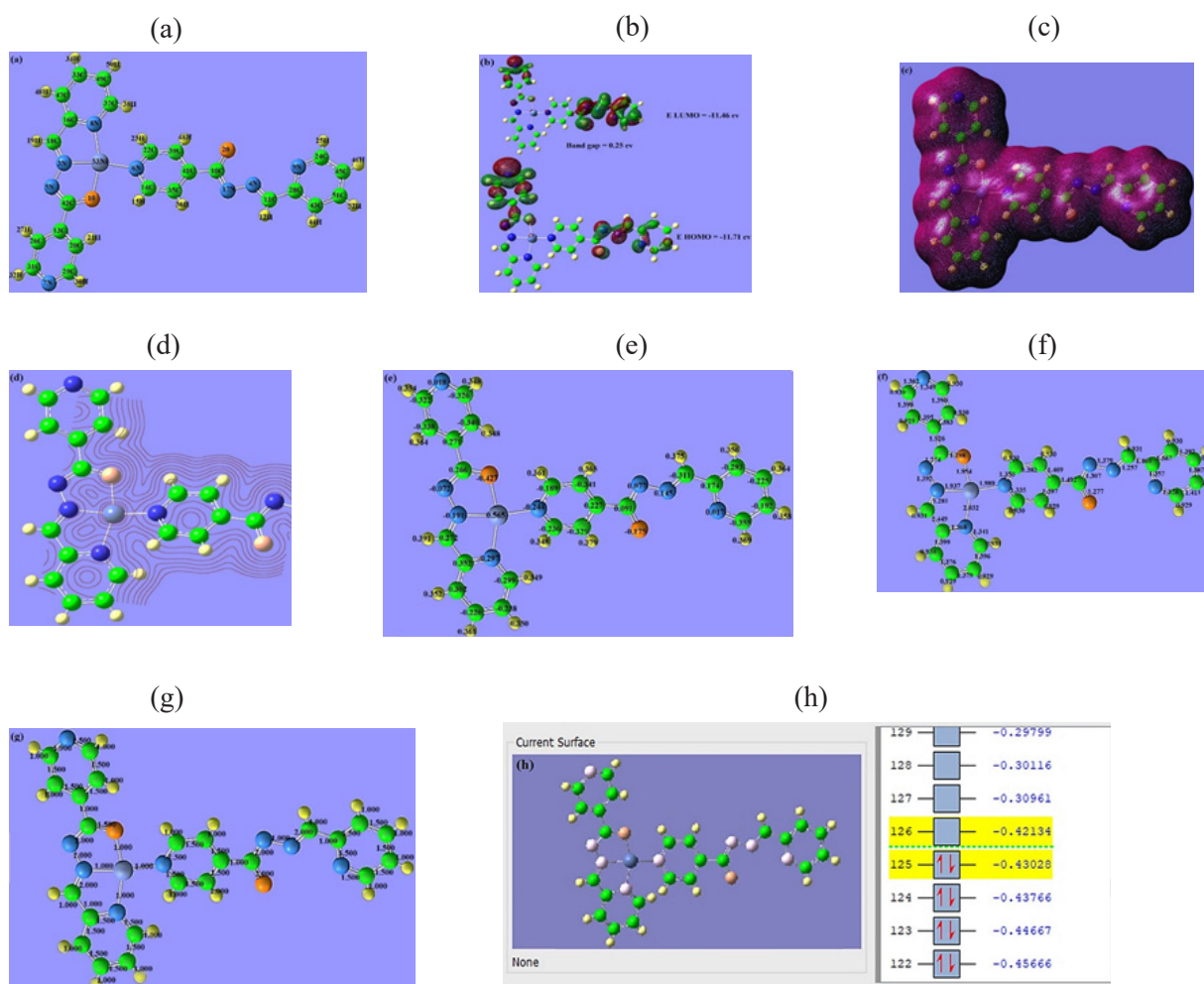


Fig 3.a) The proposed structure of the  $[\text{Ni}(\mu\text{-L})_n(\text{NO}_3)_2]$  complex. b) The shape and energy of the HOMO and LUMO boundary orbitals with the band gap of the  $[\text{Ni}(\mu\text{-L})_n(\text{NO}_3)_2]$  complex. c) Three-dimensional schematic view of the total electron density of the  $[\text{Ni}(\mu\text{-L})_n(\text{NO}_3)_2]$  complex. d) Two-dimensional schematic view of the total electron density of the  $[\text{Ni}(\mu\text{-L})_n(\text{NO}_3)_2]$  complex. e) Exhibition of partial charge by the Mulliken method. f) Bond lengths of the  $[\text{Ni}(\mu\text{-L})_n(\text{NO}_3)_2]$  complex. g) Bond orders of the  $[\text{Ni}(\mu\text{-L})_n(\text{NO}_3)_2]$  complex. h) Diamagnetic System  $[\text{Ni}(\mu\text{-L})_n(\text{NO}_3)_2]$  complex.

In Figs. 3f and 3g, the bond lengths and bond orders of the  $[\text{Ni}(\mu\text{-L})_n(\text{NO}_3)_2]$  complex are shown, respectively. In Fig. 3f, the bond lengths of the ligand increase compared to the free state due to the partial charge transportation and coordination formation. According to Fig. 3h and the calculation results, a diamagnetic square planar system is predicted for the  $[\text{Ni}(\mu\text{-L})_n(\text{NO}_3)_2]$  complex.

The FT-IR spectrum shows the characteristic peaks of 2-pyridinecarboxaldehyde at  $1700\text{ cm}^{-1}$  (Fig. 4a), and isonicotinohydrazide at  $1678\text{ cm}^{-1}$  (Fig. 4b); which is attributed to the C=O (amide) and C=O (aldehyde), respectively. The FT-IR spectra of the ligand (L) (Fig. 4c) show absorption bands in the  $3382$  and  $1663\text{ cm}^{-1}$ , which is attributed to the N-H, stretching vibrations and imine groups bands. The stretching vibration bands of N-H indicates the absence of tautomerization enol-ketone of ligand, and a ligand is a ketone form. The FT-IR spectrum of the ligand (L) has a series of strong to medium bands at  $1439\text{ cm}^{-1}$  and  $2993\text{ cm}^{-1}$ , which can be attributed to the -CH vibrational mode, and -CH stretching mode respectively. By comparing the spectra of isonicotinohydrazide, 2-pyridinecarboxaldehyde, and L synthesized a Schiff base is confirmed.

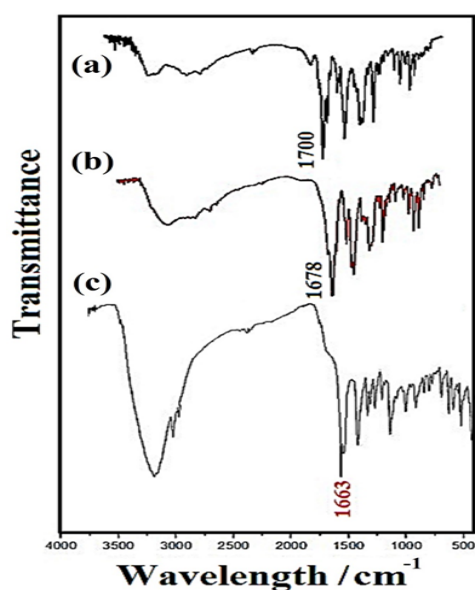


Fig.4. FTIR spectra of a) 2-pyridinecarboxaldehyde, b) isonicotinohydrazide, and c) the Schiff base.

Fig. 5 shows the typical FT-IR spectra of the  $[\text{Ni}(\mu\text{-L})_n(\text{NO}_3)_2]$  complex. The FT-IR spectrum of  $[\text{Ni}(\mu\text{-L})_n(\text{NO}_3)_2]$  complex, the absorption band at  $1616\text{ cm}^{-1}$  can be attributed to the C=N bond. Also, the assigned band for the C=N bond at  $1,663\text{ cm}^{-1}$  in the Schiff base shifts to  $1616\text{ cm}^{-1}$  at  $[\text{Ni}(\mu\text{-L})_n(\text{NO}_3)_2]$ . This shift towards lower frequencies represents the coordination of the ligand to the metal. The band located at  $1120\text{ cm}^{-1}$  corresponds to the C-O band. The band existing in  $1057\text{ cm}^{-1}$  confirms that the electron pair repulsion of the nitrogen atoms decreases because of the coordination of the ligand to the metal. The band located at  $1,363\text{ cm}^{-1}$  corresponds to free  $\text{NO}_3$  [18]. The FT-IR spectrum of the  $[\text{Ni}(\mu\text{-L})_n(\text{NO}_3)_2]$  complex, furthermore the characteristic peak of L, has a strong to medium bands at  $438$  and  $549\text{ cm}^{-1}$  that are attributed to the (Ni-N) and (Ni-O) bonds, respectively. The evaluation of the FT-IR spectra of the free ligand (L), and its Ni(II) complex (Fig. 4c and 5, respectively) enables the confirmation of the coordination mode for the ligand to the metal.

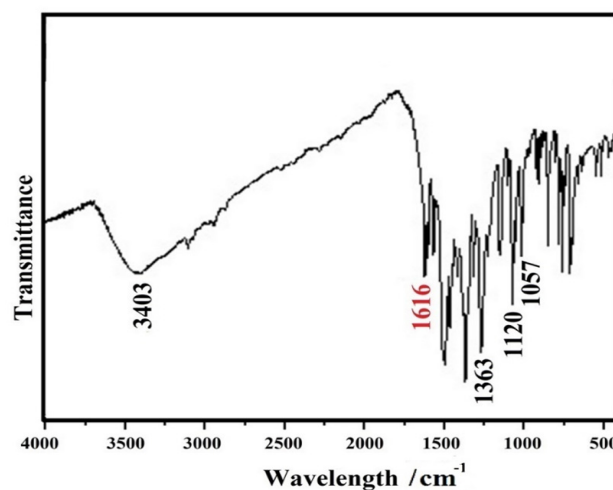


Fig. 5. FTIR spectra of  $[\text{Ni}(\mu\text{-L})_n(\text{NO}_3)_2]$ .

The FT-IR of the modified NiO-GDC is shown in Fig. 6. The absorption band at  $692\text{ cm}^{-1}$  is assigned to the metal-oxygen (Ce-O and/or Gd-O) stretching vibrations [12]. In  $3,450\text{ cm}^{-1}$  we saw a broad peak cor-

responds to the O-H stretching vibration bond. The bands detected at 1,703 and 1380  $\text{cm}^{-1}$  correspond to the C=O bond and  $\text{NO}_3$  group's vibration modes.

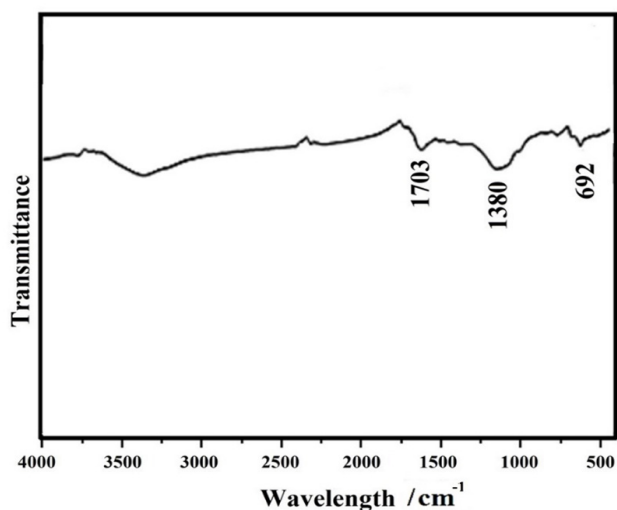


Fig. 6. FTIR spectra of modified NiO-GDC.

The Raman spectrum obtained from the  $[\text{Ni}(\mu\text{-L})]_n(\text{NO}_3)_2$  complex is shown in Fig. 7a. The type and location of the Raman spectrum bands of the  $[\text{Ni}(\mu\text{-L})]_n(\text{NO}_3)_2$  complex are given in Table 1. In the Raman spectrum, the band seen in 1646  $\text{cm}^{-1}$  relates to the imine group (C=N). Also, the assigned peak for the C=N band at 1757  $\text{cm}^{-1}$  in the Schiff base (L) (Fig. 7b) shifts to 1,646  $\text{cm}^{-1}$  in  $[\text{Ni}(\mu\text{-L})]_n(\text{NO}_3)_2$  which is in good agreement with the IR this complex spectrum. The DRS Spectroscopy of the  $[\text{Ni}(\mu\text{-L})]_n(\text{NO}_3)_2$  (Fig. 8) has a broad absorption band at 344 nm, which is related to LMCT. This transition follows both the rules of the laport and the spin permissible, so it is highly intense. The absorption bands observed in the visible region of the spectrum are usually related to the d-d transitions, which are weaker than the LMCT transition. The essential adsorption bands of the  $[\text{Ni}(\mu\text{-L})]_n(\text{NO}_3)_2$  complex are shown in Table 2.

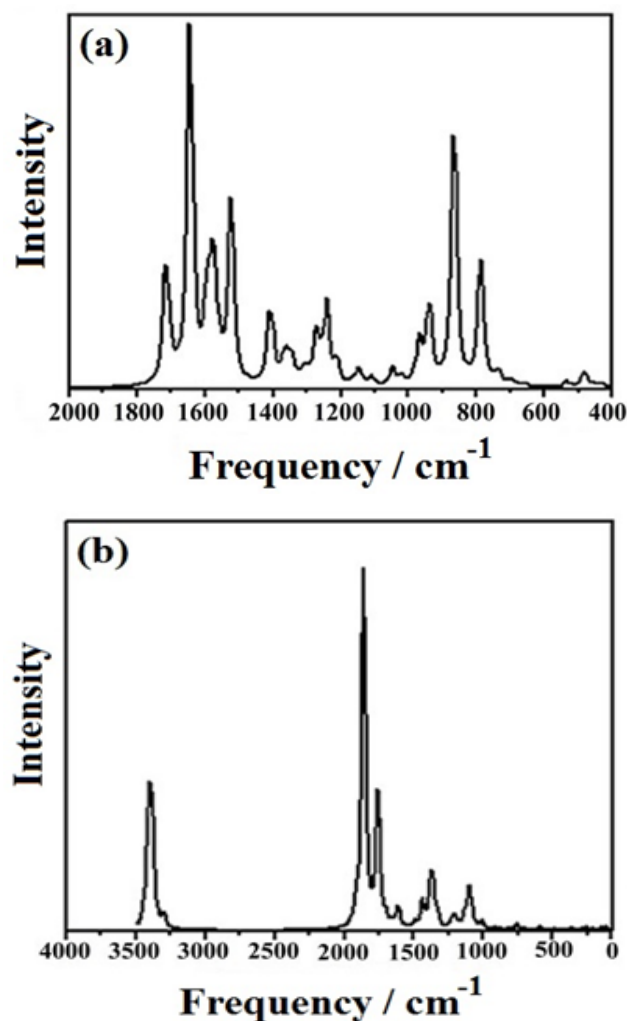


Fig. 7. Raman spectra of a)  $[\text{Ni}(\mu\text{-L})]_n(\text{NO}_3)_2$  and b) the Schiff base (L).

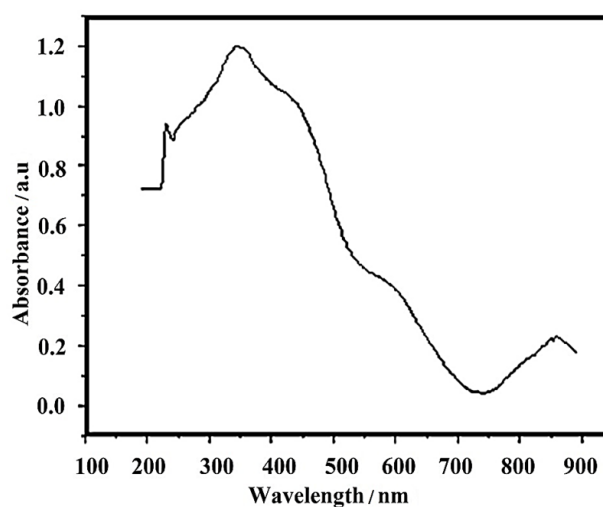


Fig.8. DRS Spectroscopy of the  $[\text{Ni}(\mu\text{-L})]_n(\text{NO}_3)_2$  complex.

**Table 1.** The type and location of the Raman spectrum bands of the  $[\text{Ni}(\mu\text{-L})]_n(\text{NO}_3)_2$  complex

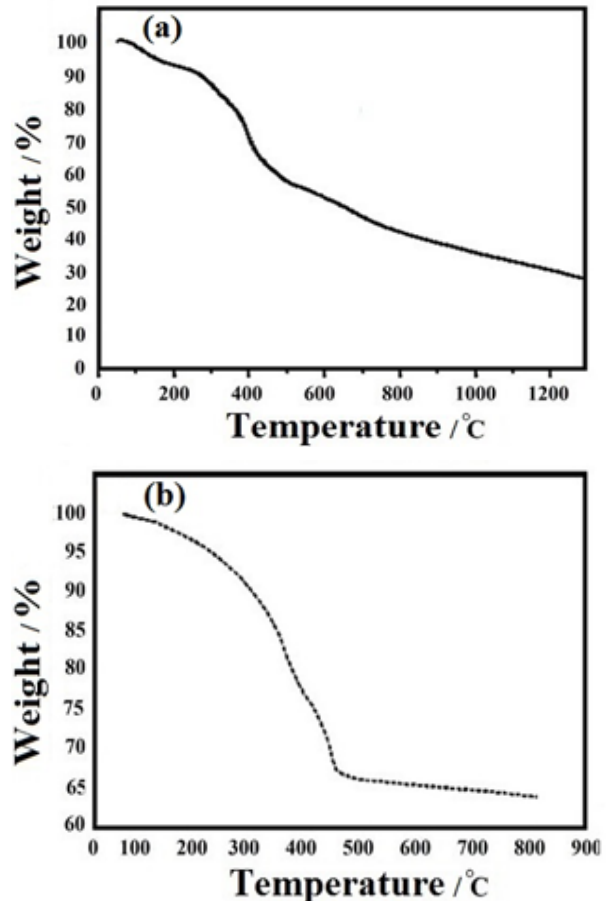
| Wavenumber / $\text{cm}^{-1}$ | Assignment    |
|-------------------------------|---------------|
| 789, 868, 1523, 1713          | Pyridine Ring |
| 1646                          | C=N           |
| 1243                          | C-O           |

**Table 2.** The most essential adsorption bands of the  $[\text{Ni}(\mu\text{-L})]_n(\text{NO}_3)_2$  complex in the DRS spectroscopy

| Wavelength / nm | Abs.  |
|-----------------|-------|
| 344             | 1.199 |
| 230             | 0.942 |
| 242             | 0.886 |
| 858             | 0.231 |
| 740             | 0.042 |

The thermal behavior of the modified NiO-GDC and  $[\text{Ni}(\mu\text{-L})]_n(\text{NO}_3)_2$  complex have been evaluated by TG/DTG characterizations, shown in Fig. 9. Its thermal stability has been consistent with our previous study [12]. To examine the thermal stability of the modified NiO-GDC, thermal gravimetric (TG) and differential thermal gravimetric analysis (DTG) were carried out at 25-1200 °C under argon flow. Fig. 9a, the weight loss for the temperature up to 200 °C is corresponding to the removal of shallow and structural water in the gel precursor and free ethylene glycol [14]. The second step corresponds to the decomposition of the inorganic and organic constituents of the precursors, such as the decomposition of the metal complex ( $[\text{Ni}(\mu\text{-L})]_n(\text{NO}_3)_2$ ). In the final step, the largest exothermic peak indicates the elimination of the remaining volatile materials, such as organic materials, nitrates, and other unwanted compounds and at the point of 1200 °C were liberated gradually. In order to test the thermal stability of the synthesized  $[\text{Ni}(\mu\text{-L})]_n(\text{NO}_3)_2$  complex, TG and DTG were carried out at a temperature range of 25-800 °C under argon (Fig. 9b). Fig. 9b; shows the first slight weight loss at 90 °C, which is related to the solvent outflow from the complex structure. The TG curve shows that the com-

plex is not melting and is stable until the temperature of 110 °C, which indicates the stability of the framework  $[\text{Ni}(\mu\text{-L})]_n(\text{NO}_3)_2$  to these temperatures.

**Fig. 9.** TG/DTG diagram of the a) modified NiO-GDC and b)  $[\text{Ni}(\mu\text{-L})]_n(\text{NO}_3)_2$  complex.

The XRD pattern of the calcined modified NiO-GDC powder at 600 °C presented in Fig. 10, identifies the fluorite-type structure (space group  $\text{fm}\bar{3}\text{m}$ ) [19]. Fig. 10; also presents the modified NiO-GDC that shows all the main reflections corresponding to (111), (200), (220), (311), (222), (400) and (420) in the scanning of range 20–90° of  $2\theta$  and no impurity peaks were observed [20, 21]. The average crystallite sizes for the modified NiO-GDC powder calcined at 600 °C was obtained 17.67- 28.28 nm based on the Scherrer equation. Also, no intermediate phase is observed in the XRD pattern of the composite show fluorite the

GDC and cubic NiO, which indicates no solid solution between GDC and NiO [22]. According to the XRD results [9] in published papers, when the calcination temperature increases, the intensity of the peak becomes sharp, and the crystallinity of the powder increases. Also, the coarsening of the particles by heat treatment sometimes occurs [9]. Here the formation of a solid solution between the GDC and NiO significantly occurs due to the smaller ionic radius of  $\text{Ni}^{2+}$  (0.69 Å) in comparison with both the  $\text{Ce}^{4+}$  (0.97 Å) and  $\text{Gd}^{3+}$  (1.053 Å) [23]. The XRD analysis of the 600 °C calcined powder reveals the complete oxidation of the Ni-metal to NiO.

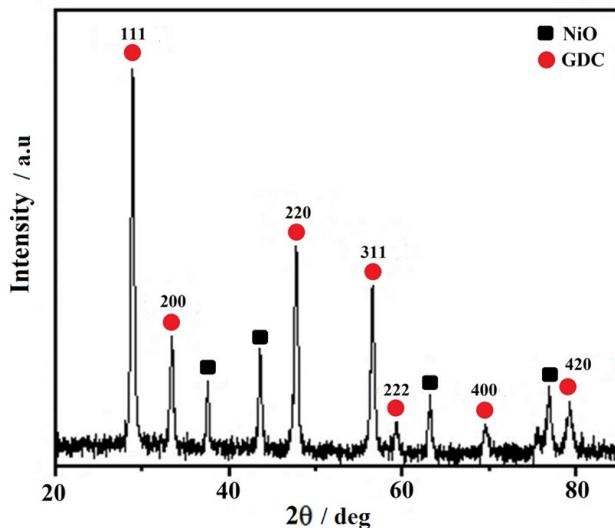


Fig.10. The X-ray powder diffraction pattern of the modified NiO-GDC

The scanning electron micrograph of the modified and conventional NiO-GDC powder is given in Fig. 11a and b. The two different phases, NiO and GDC, are distinctly identified in the micrograph and are uniformly distributed and well-connected [22]. The SEM micrograph indicates that the larger grains correspond to the GDC phases and the smaller grains to the NiO phase. It can be seen that the distribution of

NiO in the GDC matrix of the modified NiO-GDC is obtained with only a large amount of porous, spherical grains. Additionally, a comparably more porous surface with increased pore size is observed for the modified NiO-GDC sample. The porous are uniformly distributed around each grain [24, 25]. When the  $[\text{Ni}(\mu\text{-L})]_n(\text{NO}_3)_2$  complex are employed as the precursor, the SEM micrograph of the modified NiO-GDC shows a uniform structure without cracks, while the  $[\text{Ni}(\mu\text{-L})]_n(\text{NO}_3)_2$  has a different morphology with a cracked structure and sharp edges (Fig. 11c). The anode must have sufficient porosity to allow enough mass transport and to also minimize the loss of useful voltage in the cell performance [25]. The micrograph of the conventional NiO-GDC indicates only a small amount of porous, but the micrographs of the modified NiO-GDC indicate that the structure is composed of homogeneous agglomerated with large porous [12]. According to research [26], the formation of comparatively large clusters and porous in the NiO-GDC powders can be formed due to the re-agglomeration of the grains. The primary particles of the GDC and NiO with several sizes agglomerate to form large secondary particles and form a highly porous network structure [9]. The particles of the GDC and NiO are bonded together at the active contact points [3]. The TPB is attributed to the uniform distribution of the NiO and GDC grains in the NiO-GDC anodes. The large porosity in the NiO-GDC anodes led to an enlarged TPB by high-temperature sintering [27, 28], and the calcined composite anode powders caused the maximizing of the TPB length as well as high cell performance. As well, in the sol-gel process, the pore distribution and particle size were more homogeneous, smaller, and without contaminants. It is suggested that the use of the NiO-GDC-composite powders along with the improvement of its surface, could improve anode performance and increase the length of the TPB, which may increase the electrochemical performance half-cell of the SOFC.

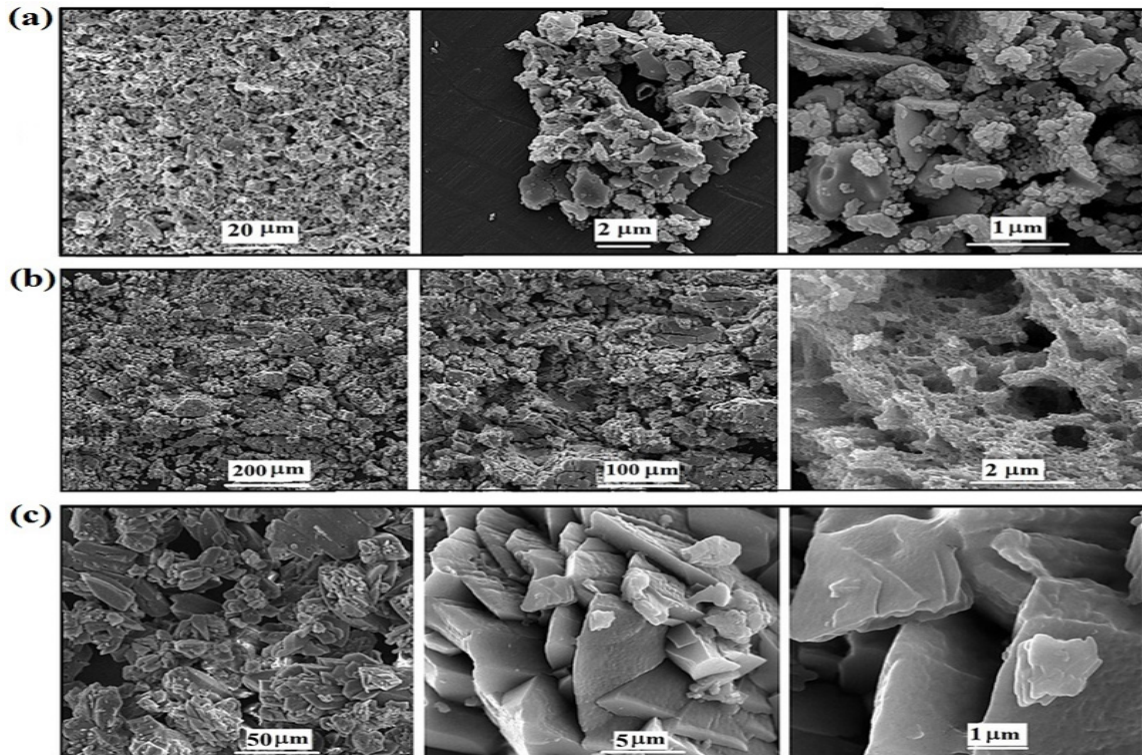


Fig. 11. SEM micrograph of the a) modified NiO-GDC, b) conventional NiO-GDC powders, and c)  $[\text{Ni}(\mu\text{-L})]_n(\text{NO}_3)_2$  complex.

To further identify the NiO-GDC particles, the TEM micrograph of the modified NiO-GDC powder synthesized by the sol-gel method is shown in Fig. 12. The TEM analysis revealed that the particles consisted of a nano-composite of small NiO and GDC particles, homogeneously distributed all over the composite. In the modified NiO-GDC, the NiO particles were large spherical and non-spherical particles, while the GDC particles were small spherical particles that created aggregates due to their high surface area [12]. The particles of the GDC and NiO are bonded together at the active contact points. In Fig. 11, due to the fact that the magnification of the images are micron, the particles of NiO and GDC cannot be distinguished from each other, but in the TEM image, Fig. 12, the dark and light particles represent two types of particles, which include NiO and GDC. It seems that the dark areas are GDC and the light areas are NiO, considering that the amount of light areas are more than dark parts (60 % NiO, 40 % GDC). It seems that

the use of the new nickel complex in the modified NiO-GDC caused uniform doping of the surface structure.

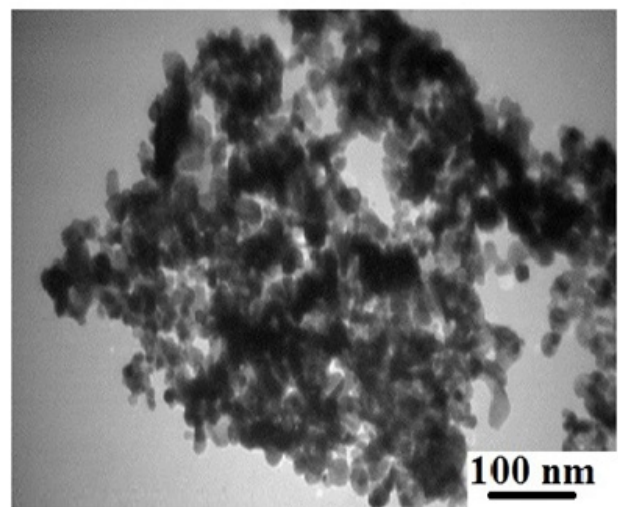


Fig. 12. The TEM micrograph of the modified NiO-GDC powder.

The nitrogen adsorption analysis revealed a differentiated structure for the conventional and modified powders obtained (Fig. 13). The modified anode powder presented; showed an average hysteresis loop when the relative pressure was higher than 0.5 by the gap between the absorbed volume of  $N_2$  adsorption and desorption isotherm [29]. The isotherm of the modified NiO-GDC indicated that it has a mesoporous structure. Hysteresis, appearing in the multilayer range of physisorption isotherms is usually associated with mesoporous structures [30]. The conventional

NiO-GDC showed a hysteresis loop smaller than that of the modified NiO-GDC, which is similar to type II,  $N_2$  adsorption/desorption isotherms of non-porous or macro-porous material; therefore, it confirmed and gave the new precursor  $[Ni(\mu-L)]_n(NO_3)_2$  resulted in a better powder than the one prepared by the  $Ni(NO_3)_2 \cdot 6H_2O$ , that gives a more significant surface area with continuous networks of each phase, including nickel, GDC and pores to perform electrochemical reactions.

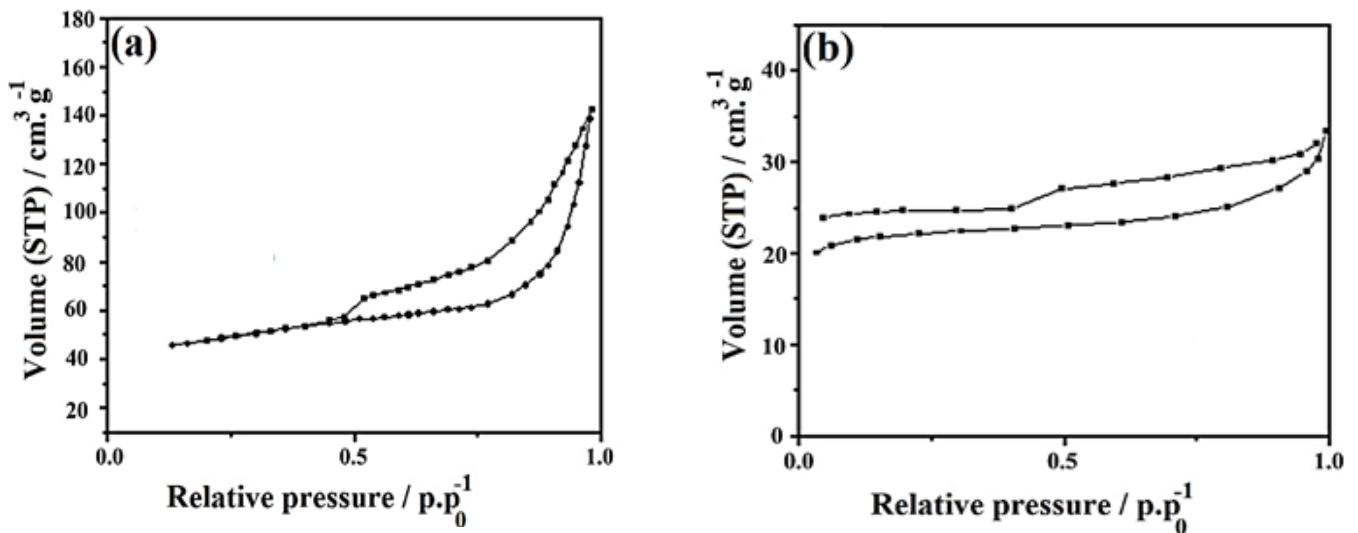


Fig. 13. Adsorption-desorption isotherm of the a) modified NiO-GDC and b) conventional NiO-GDC powders synthesized by the sol-gel method.

Fig. 14 shows the Nyquist plots for both the conventional and modified NiO-GDC anodes for the hydrogen oxidation reaction in the humidified  $H_2/N_2$  at 650, 750 and 800 °C. It has been reported that the performance of a porous anode electrode is mainly affected by the interface resistance of the electrode which is itself dependent on both the electrical conductivity and microstructure of the electrode [31]. Generally, the essential requirements for an anode electrode are adequate catalytic activity, adsorption of the hydrogen molecule to the electrode surface and desorption of the products, gas diffusion through the pore channels, and electronic conductivity of anode materials [31]. Typically, the electronic conductivity and the

anode's microstructure are improved by the reduction of Ni-based anodes resistance. In Fig. 14, two semicircles are observable in the impedance spectra of both the conventional and modified NiO-GDC anodes at high and low frequencies which are mainly attributed to the resistance against the charge transfer and gas diffusion through the electrode porous, respectively. The value of the total polarization resistance is a summation of the charge transfer and gas diffusion resistances which are measured from the data in the Nyquist plots. Fig. 14 revealed that the modified NiO-GDC anode showed a lower anodic polarization resistance ( $0.83 \Omega \cdot cm^2$ ) compared to the conventional NiO-GDC anode ( $1.54 \Omega \cdot cm^2$ ) at 800 °C. The impedance spec-

trum is analyzed according to the theory of the porous electrode, and the ion transport of the electrode is controlled by the ionic conductivity of the framework of the theory of the porous electrode. At 800 °C, the microstructure of NiO/GDC changes and creates more porosity. In fact, with the increase in temperature up to 800 °C, the crystalline structure changes and tetrahedral holes are created inside the structure, and then the gas phase diffusion process increases significantly. At temperatures of 650 and 750 °C, this structural change has not yet occurred and there is not enough porosity for gas diffusion [32]. The augmentation can explain the low polarization resistance of the prepared sample using the novel nickel complex in the Ni-Ni contact, and consequently, better electronic conduction. The improved Ni-Ni particle connectivity originates from the improved elastic property of the modified NiO-GDC with the new nickel complex, which in turn increases the ordering of the network structure of the NiO-GDC powder and ultimately improves the particle connectivity in the electrode. It is highly likely that higher Ni-Ni contact improves the interconnection between the metal and metal oxide particles in the modified NiO-GDC [33]. Moreover, the modified NiO-GDC, with the addition of  $([\text{Ni}(\mu\text{-L})]_n(\text{NO}_3)_2)$ , resulted from the improved porosity during the sintering, and this improved the gas diffusion through the porous and consequently lowered the diffusion impedance resistance. Therefore, both the diffusion and charge transfer resistances were strongly affected by the precursors in the NiO-GDC samples. Also, this difference observed in the NiO-GDC samples could be attributed to the difference in gas diffusion properties owing to the microstructure including the pore size, total porosity, and tortuosity of the anode pore channels [8]. As well, the synthesis of the NiO-GDC by a one-pot glycine nitrate process indicated that the resistance of the modified anode powder decreased from 1.29 to 0.76  $\Omega\cdot\text{cm}^2$  at 800 °C [9]. In another research that optimized the surface of the structure with ball mill grinding, the charge transfer with a finer-grained

microstructure was enhanced, and the polarization resistance decreased [11]. In similar research, in order to optimize this microstructure, the NiO-GDC nano-powders were obtained by a one-step chemical method [34]. The results of the research by Grilo et al. [34] showed that by using the one-step method, an ideal microstructure with homogeneous phase distribution was created. Therefore, in the conventional NiO-GDC, the connection between the NiO and GDC was weak, but through the addition of  $([\text{Ni}(\mu\text{-L})]_n(\text{NO}_3)_2)$  to the modified NiO-GDC, the NiO; and GDC were homogeneously distributed, and their interaction enhanced the electrical conductivity.

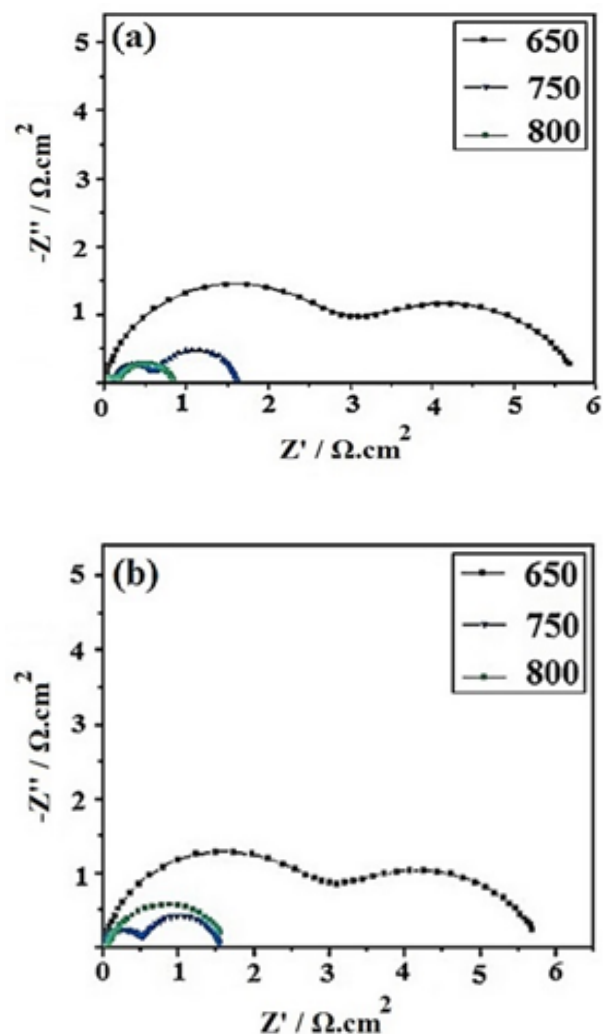


Fig.14. Polarization resistance values determined at temperatures of 650, 750, and 800 °C for the a) modified NiO-GDC and b) conventional NiO-GDC powders.

#### 4. Conclusion

Intending to develop high-performance SOFC anodes, this study successfully investigated the electrical properties of the prepared NiO–GDC composites. A comparison of the NiO–GDC anode prepared with the new precursor and the NiO–GDC synthesized from metal nitrate salt showed that the modified NiO–GDC had a porous microstructure composed of uniformly distributed and well-connected constituent grains. The modified microstructure of the NiO–GDC could improve the TPB area between the H<sub>2</sub> gas, Ni (electronic conductor), and GDC (electrolyte and ionic conductor). The results of the electrochemical analysis for the NiO–GDC samples revealed that the modified NiO–GDC anode had a lower anodic polarization resistance than that of the conventional NiO–GDC anode at 800 °C, which showed the excellent behavior of the electrochemical performance. Consequently, the results showed that the modified NiO–GDC anode in this study could be a promising material for use in anodes for IT-SOFCs.

#### Acknowledges

The authors are grateful to the Iranian Research Organization for Science and Technology (IROSt), University of Tehran (UT), and Iranian National Science Foundation (INSF) for their support in this study.

#### References

- [1] In WonChoi, WonjongYu, Myung SeokLee, Sang-bongRyu, Yoon HoLee, Suk WonCha, Gu YoungChho, *Journal of Power Sources*, Volume 531, 30 May 2022, 231320
- [2] YosukeKomatsu, AnnaSciazko, YasuhikoSuzuki, ZhufengOuyang, ZhenjunJiao, NaokiShikazono, *Journal of Power Sources*, Volume 516, 31 December 2021, 230670
- [3] S.A.N.França Junior, A.L.R.Souza, L.B.Cruz, F.Vaz, A.Ferreira, F.Bohn, W.Acchar, M.A.Correa, *Ceramics International*, 48 (2022) 20260-20265.
- [4] T. Arjomandbigdeli, Z. Isapour, A. Malek Khachaturian, M. Golmohammad, *Iranian J Hydrogen and fuell cell*, 8 (2021) 43-49.
- [5] A. Ghani Harzand, A. Nemat, M. Golmohammad, A. Malek Khachaturian, *Iranian J Hydrogen and fuell cell* 8 (2021) 51-58.
- [6] Z. Shao, W. Zhou, Z H. Zhu, Z H, *Progress in Materials Science*, 57 (2012), 804-874.
- [7] S. Park, Ch. Woong Na, J. Ahn, R. Song, J. Lee, *Journal of Asian Ceramic Societies*, 2 (2014), 339-346.
- [8] T. Hosseinzadeh Sanatkar, A. Khorshidi, E, Sohoul, J. Janczak, *Inorganic Chemica Acta*, 506 (2020), <https://doi.org/10.1016/j.ica.2020.119537>.
- [9] S. Bhattacharya, M. Ray, *Inorganic Chemica Acta*, 502 (2020), <https://doi.org/10.1016/j.ica.2019.119338>.
- [10] Y. Daeil, Su. Qing, W. Haiyan, M. Arumugam,

- Phys.Chem. Chem. Phys, 15 (2013), 14966-14972.
- [11] F. Sadat Torknik, M. Keyanpour-Rad, A. Maghsoudipour, G. Man Choi, *Ceramics International*, 40 (2014), 1341-1350
- [12] S. Ghamari, M. Ranjbar, M. Nabitabar, *J Sol-Gel Sci Technol*, 81 (2017), 236-246.
- [13] B. Shaabani, A. Akbar, S. Sadat, and Z. Shaghghi, *Polyhedron*, 49 (2013), 61-66.
- [14] A. Zarkov, A. Stanulis, T. Salkus, A. Kezionis, V. Jasulaitiene, R. Ramanauskas, S. Tautkus, A. Kareiva, *Ceramics International*, 42 (2016), 3977-3988.
- [15] A. Babaei, S. Ping Jiang and Li. Jian, *Journal of The Electrochemical Society*, 156 (2009), 1022-1029.
- [16] M. Mousavi, V. Béreau, C. Desplanches, C. Duhayon, and J.-P. J. C. C. Sutter, *Chem. Commun*, 46 (2010), 7519-7521.
- [17] M. Rivera-Jiménez, A. J. J. M. Hernández-Maldonado, and M. Materials, *Microporous and Mesoporous Materials*, 116 (2008), 246-252.
- [18] Nakamoto, Kazuo, *Infrared and Raman Spectra of Inorganic and Coordination Compounds*, John Wiley & Sons, Inc., Hoboken, New Jersey, 2009.
- [19] J. Martinez, R. Meneses, C. Silva, *Materials Science Forum*, 182 (2014), 798-799.
- [20] M. Brant, F. Possa, F. Lameiras, *Materials Science Forum*, 624 (2005), 498-499.
- [21] S. Dikmen, P. Shuk, M H. Greenblatt, *Solid State Sciences*, 4 (2002), 585-590.
- [22] A U. Chavan, A P. Jamale, S P. Patil, C H. Bho-sale, S R, Bharadwaj, P S, Patil, *Ceramics International*, 38 (2012), 3191-3196.
- [23] R. Ghelich, M. Keyanpour-Rad, A. Youzbashi, Z. Khakpour, *Materials Research Innovations*, 19 (2015), 44-50.
- [24] D. Changsheng, S. Kazuhisa, M. Junichiro, H. Toshiyuki, *ELSEVIER*, 38 (2012), 85-92.
- [25] S. Kim, H. Moon, S. Hyun, J. Moon, J. Kim, H. Lee, *Solid State Ionics*, 178 (2007), 1304-1309.
- [26] M. Chourashiya, L. Jadhav, "Synthesis and characterization of 10% Gd doped ceria (GDC) deposited on NiO-GDC anode-grade-ceramic substrate as half cell for IT-SOFC," *international journal of hydrogen energy*, 36 (2011), 14984-14995.
- [27] T. Suzuki, Z. Hasan, Y. Funahashi, T. Yamaguchi, Y. Fujishiro, M. Awano, *Science*, 325 (2009), 852-855.
- [28] K H. Ng, S. Lidiyawati, MR. Somalu, R. Muchtar, H. Rahman, *Procedia Chemistry*, 19 (2016), 267-274.
- [29] S. Ahn, H. Koo, S. Bae, I. Chang, S. Cha, Y. Yoo, Ch. Park, *Journal of Nanoscience and Nanotechnology*, 14 (2014), 8117-8121.
- [30] K. Sing, D. Everett, R. Haul, L. Moscou, R. Pierotti, J. Rouquerol, T. Siemieniewska, *Pure & Appl.Chem.*, 57 (1984), 603-619.
- [31] J. Ayawanna, D. Wattanasiriwech, S. Wattanasiriwech, K. Sato, *Energy Procedia*, 34 (2013), 439-448.
- [32] T. Jacobsen, P.V. Hendriksen, S. Koch, *Diffusion*

and conversion impedance in solid oxide fuel cells, *Electrochim, Acta* 53 (2008), 7500-7508.

[33] B. Farrell, S. Linic, *Applied Catalysis B: Environmental*, 183 (2016), 386-393.

[34] J. Griloa, C. Moura, D. Macedo, S. Rajesh, F. Figueiredo, Marques. F, *Ceramics International*, 43 (2017), 8905-8911.